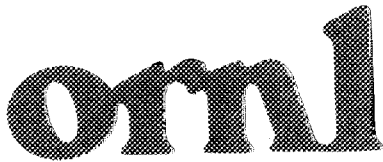


MARTIN MARIETTA ENERGY SYSTEMS LIBRARIES



3 4456 0263010 6

ORNL/TM-10421

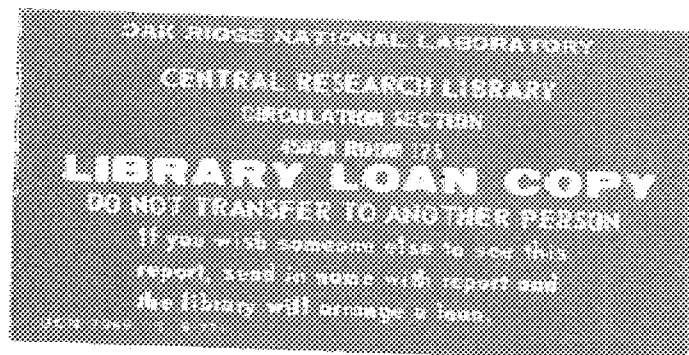


OAK RIDGE
NATIONAL
LABORATORY



Evaluation of a Digital Optical
Ionizing Radiation Particle
Track Detector

S. R. Hunter



OPERATED BY
MARTIN MARIETTA ENERGY SYSTEMS, INC.
FOR THE UNITED STATES
DEPARTMENT OF ENERGY

Printed in the United States of America. Available from
National Technical Information Service
U.S. Department of Commerce
5285 Port Royal Road, Springfield, Virginia 22161
NTIS price codes—Printed Copy: A04; Microfiche A01

This report was prepared as an account of work sponsored by an agency of the United States Government. Neither the United States Government nor any agency thereof, nor any of their employees, makes any warranty, express or implied, or assumes any legal liability or responsibility for the accuracy, completeness, or usefulness of any information, apparatus, product, or process disclosed, or represents that its use would not infringe privately owned rights. Reference herein to any specific commercial product, process, or service by trade name, trademark, manufacturer, or otherwise, does not necessarily constitute or imply its endorsement, recommendation, or favoring by the United States Government or any agency thereof. The views and opinions of authors expressed herein do not necessarily state or reflect those of the United States Government or any agency thereof.

Evaluation of a Digital Optical Ionizing
Radiation Particle Track Detector

S. R. Hunter
Health and Safety Research Division
Oak Ridge National Laboratory
Oak Ridge, Tennessee 37831

Date Published: June 1987

OAK RIDGE NATIONAL LABORATORY
Oak Ridge, Tennessee 37831
Operated by
MARTIN MARIETTA ENERGY SYSTEMS, INC.
for the
U.S. Department of Energy
Under Contract No. DE-AC05-84OR21400

MARTIN MARIETTA ENERGY SYSTEMS LIBRARIES



3 4456 0263010 6

TABLE OF CONTENTS

ACKNOWLEDGMENT		v
ABSTRACT		vii
CHAPTER		
1	INTRODUCTION	1
	Original Dosimeter Concept	2
	Limitations in the Original Dosimeter Concept	2
2	SURVEY OF POTENTIAL DOSIMETER CONCEPTS.....	4
	Basic Radiation Counters	4
	Ionization and Drift Chambers	5
	Position Sensitive Proportional Counters	6
	Optical Ionizing Radiation Detectors -	
	Spark Chambers	7
	Streamer Chambers	8
	Gas Scintillation Detectors	9
	Conclusions	9
3	OPTICAL IONIZING RADIATION DETECTOR.....	10
	Optical Detector Operation	10
4	DETECTOR DESIGN CRITERIA.....	14
	Photon Gain Requirements	15
	AC Electric Field Requirements	17
	Avalanche Growth	19
5	EXAMPLE DETECTOR RESOLUTION AND SENSITIVITY CALCULATIONS...	22
	N ₂ as a Counting Gas	22
6	CONCLUSIONS AND RECOMMENDATIONS.....	26
	Further Improvements in Detector Resolution	
	and Sensitivity	26
	Advantages of the Optical Detector Concept	28
REFERENCES.....		30

ACKNOWLEDGMENT

This research was sponsored by the Office of Health and Environmental Research, U.S. Department of Energy, under contract DE-AC05-84OR21400 with Martin Marietta Energy Systems, Inc.

Evaluation of a Digital Optical Ionizing
Radiation Particle Track Detector

S. R. Hunter

ABSTRACT

An ionizing radiation particle track detector is outlined which can, in principle, determine the three-dimensional spatial distribution of all the secondary electrons produced by the passage of ionizing radiation through a low-pressure (0.1 to 10 kPa) gas. The electrons in the particle track are excited by the presence of a high-frequency AC electric field, and two digital cameras image the optical radiation produced in electronic excitation collisions of the surrounding gas by the electrons. The specific requirements of the detector for neutron dosimetry and microdosimetry are outlined (i.e., operating conditions of the digital cameras, high voltage fields, gas mixtures, etc.) along with an estimate of the resolution and sensitivity achievable with this technique. The proposed detector is shown to compare favorably with other methods for obtaining the details of the track structure, particularly in the quality of the information obtainable about the particle track and the comparative simplicity and adaptability of the detector for measuring the secondary electron track structure for many forms of ionizing radiation over a wide range of energies.

CHAPTER 1

INTRODUCTION

A concept has recently been developed for a new approach to neutron dosimetry in which digital, rather than analog, ionization measurements can be made on charged-particle recoil tracks in an ionization chamber counting gas (Bo86,87; Tu85a,b). Whereas current methods utilize tissue-equivalent instruments and measurements on pulse height and shape to infer neutron dose and dose equivalent, the new method seeks to register a charged-particle track by measuring the number of electrons it produces in given subvolumes of a chamber gas. The track is thus characterized by a set of integers associated with each volume element. A digital detector can measure both the track length and the energy deposition by observing the production of the secondary electrons in the path of a neutron recoil ion, enabling the identity of the recoil ion, as well as its energy and LET, to be established. The ultimate detector of this type would, in principle, accurately measure the three-dimensional spatial distribution of every secondary electron produced in the gas by the passage of the ionizing radiation. Measurement of the W value for each track becomes possible with a detector of this type. Such an approach to particle track analysis can

have further considerable applications in the field of microdosimetry, for example (Tu85a). Similarly, secondary electron δ -ray tracks would also be directly observable as would the tracks produced by other forms of ionizing radiation (e.g., α , β , γ , and X rays and high-energy laser beams). The applications in which a detector of this nature can be used are principally limited by the resolution and sensitivity with which the particle track can be observed.

Original Dosimeter Concept

The original device suggested for proof of principle envisioned a 10 cm x 10 cm x 10 cm ionization chamber (the chamber contained methane gas surrounded by walls of polyethylene thereby satisfying the Bragg-Gray principle), subdivided electronically into a cubic array of 1000 subvolumes of size 1 cm³ each (Bo86,87; Tu85a,b). A charged recoil particle (in this chamber, the recoil particles are either protons or carbon ions), produced by a neutron interaction in the chamber wall, enters the chamber gas. Figure 1 shows the three-dimensional coordinates of every subexcitation electron produced by (a) a 500-keV recoil proton and (b) an 80-keV recoil carbon ion calculated by a charged particle transport code (Bo86,87). The ions are collected by a 10 x 10 array of proportional counters at the bottom of the chamber, and the track is thus characterized by 1000 integers, most of which are zero, since only those volume elements in the immediate vicinity of the track have ionized gas molecules.

Limitations in the Original Dosimeter Concept

This detection scheme and associated signal unfolding algorithm was found to successfully unfold the neutron dose and dose equivalent from the digital information for protons and carbon ions in the MeV range.

At lower energies (\lesssim few hundred keV) however, the carbon response was depressed (e.g., the carbon recoil ion track shown in Fig. 1b) with both the LET and dose equivalent being considerably underestimated. The underestimation was traced to the unfolding algorithm's overestimate of the average track length due to the relatively poor spatial resolution of the simulated detector (Bo86,87). Increased spatial resolution ($\lesssim 1 \text{ cm}^3$) would greatly increase the accuracy of neutron dose and dose equivalent for low-energy protons and carbon ions from these calculations. The detection of details in the track structure (e.g., δ -ray tracks and fluctuations in W values) also become possible with increasing spatial resolution (Tu85a).

An ionizing particle track detector is outlined in this report that can, in principle, determine the three-dimensional spatial distribution, with good resolution ($\lesssim \text{mm}^3$), of the secondary electrons produced in a gas by the passage of ionizing radiation. The present scheme is an optical method where the locations of the secondary electron tracks are imaged by the radiation produced in the excitation of the surrounding gas by the electrons in the particle track. This is in contrast to the needle detector concept which was the subject of analysis in the previous studies of the digital track structure approach (Bo86,87; Tu85a,b).

CHAPTER 2

SURVEY OF POTENTIAL DOSIMETER CONCEPTS

There are several competing techniques for track structure analysis, most of which have been developed for use in the fields of high energy and elementary particle physics. These radiation detectors have specific advantages and disadvantages when used in these applications but appear incapable at the present time of generating as much information about the secondary electron distribution as the optical technique which is described in the next section. The most promising gaseous ionizing radiation detectors which could potentially be useful in dosimetric applications can be divided into two broad categories; those which measure the displacement current in the device due to the motion of electrons and ions under the influence of an external electric field and those which detect the optical radiation produced in excitation of the gas by the electrons in the particle track.

Basic Radiation Counters

The simplest devices are the well-known cylindrical geometry Geiger-Mueller, proportional and ionization counters which differ from

each other principally in the field that is applied between the cylindrical cathode and wire anode. These devices are only capable of measuring the total count rate (Geiger-Mueller counter) or the amount of charge in each ionization event for weakly ionizing (proportional counter) or strongly ionizing (ionization chamber) events. These comparatively simple devices were the subject of an intensive developmental effort beginning in the late 1960s when it was realized that the spatial distribution, as well as the energy content of the ionizing radiation, could be determined with devices of this type (e.g., Ch68; Fa80). In general, these chambers have a planar geometry and contain one or more wire electrode arrays which act to define the shape of the electric fields within the device, are used as timing electrodes, or are used as charge collection anodes depending on the type of device (Ch79; Fa80).

Ionization and Drift Chambers

The most basic of these detectors is the planar ionization chamber, where the applied fields are low and gas multiplication does not occur. Using delay line techniques in conjunction with fine wire sensing grids (Bo68), it is possible to determine the total amount of ionization, the depth of the track, and angular position of the track in the chamber for a heavily ionizing particle (Fu79). In neutron spectroscopy applications, however, the counter should be capable of determining not only the energy of the recoil ions but also the angle of recoil with respect to the direction of entry of the neutron. In practice, this has proved to be a difficult problem with conventional counters (Fu79). For more weakly ionizing radiation, proportional counting techniques must be used, and multiwire proportional and drift chambers have been developed

for this purpose (Ch68). These devices, when operated at relatively low gain [$<10^3$ to 10^4 , the gain is limited by space-charge saturation (Fa80)], are capable of high spatial resolution (uncertainty $<100 \mu\text{m}$) in the two-dimensional plane parallel to the electrode surfaces and are also able to measure the total charge in the particle track. At high electron gains the pulse amplitude is limited by space-charge saturation effects leading to Geiger-Mueller-type operation or to streamers followed by gas breakdown between the electrodes (Ch79). A more versatile version of this instrument is the multiwire drift chamber. In this device, the electrons produced by the ionizing radiation drift away from their initial position of production under the influence of a low electric field to a wire anode array, where they are detected. If the time of creation is accurately known, then the time interval between creation and detection of the electrons is a measure of the initial position of the particle track enabling the direction of the primary ionizing particle through the detector to be recorded in three dimensions. Considerable developmental work (in terms of the best choice of counter gas mixtures, electrode geometries, high-speed electronics, etc.) has been invested in this type of detector in recent years (e.g., see reviews by Sa78; Ch79; Fa80; Va86), and spatial resolutions $\lesssim 50 \mu\text{m}$ with timing accuracies of ≈ 1 to 5 ns have been achieved using these detectors (Va86).

Position Sensitive Proportional Counters

An alternate version of the position-sensitive, proportional chamber is the needle chamber (Gr74a,b) in which the wire anode array is replaced by a two-dimensional array of needles. This chamber concept has been the subject of analysis in the previous paper (Bo87) and other

studies aimed at identifying the critical detector requirements in neutron dosimetry applications (Tu85a,b). The two-dimensional coordinates of the secondary electron-charge distribution parallel to the needle array plane and the total charge in the electron track can be measured at the needle array. If the time of production of the electron track is known accurately, then the arrival time spectra of the charge at the needle array will be a measure of the third coordinate. This detector concept has been the subject of several studies (Gr74a,b; Fu75; Sa75; Co80) and chambers containing over 1000 needles have been made with spatial resolutions ≤ 1 mm (Co80). These chambers have been operated at high gain (10^7 to 10^8 , Co80) and, consequently, have not provided information about the initial electron population density. Simple pin detectors have been operated at lower gain (10^3 to 10^6) in a proportional mode and have shown good two-dimensional (resolution < 1 mm) imaging of the electron track (Ba85a,b).

Optical Ionizing Radiation Detectors - Spark Chambers

The second broad category of detectors measures the amount of optical radiation produced in the device, either by the primary ionizing radiation (e.g., gas and solid scintillator detectors) or by secondary electron-molecule excitation collisions when the electrons are accelerated to energies considerably in excess of thermal and collide inelastically with the surrounding atoms or molecules to produce optical radiation and additional electrons by ionization. The simplest of these devices is the spark chamber (Ch57,70; Fu59; Co60; Fa80) which consists of a stack of closely spaced parallel plates or wires with a constant high voltage field applied between these electrodes. The passage of an ionizing particle through the device, approximately perpendicular to the

plane of the electrodes, produces secondary electrons in the gas which rapidly grow to avalanche proportions (10^9 to 10^{10} electrons) and ultimately produce a spark between the consecutive electrodes. The imaging of these discharges reveals the location of the track through the device. These types of detectors are no longer in use due to their poor resolution and low counting rate (Fa80).

Streamer Chambers

An alternate track visualization concept is the streamer chamber, where the secondary electron avalanche growth in the track is halted after a finite time interval (5 to 20 ns) before the streamer has achieved a significant spatial extension (>1 to 5 mm) but is still long enough such that sufficient optical radiation is produced to visualize the avalanche (i.e., high enough electron gain $>10^8$). An external scintillator records the passage of the ionizing radiation through the detector and is used to trigger a pulsed high voltage source which produces a high electric field across the detector electrodes. The electric field is of sufficient duration and magnitude to cause high gas amplification, but the high voltage pulse is short enough such that gas breakdown does not occur. These detectors were developed in the early 1960s (Ch64; Do64; Bu65; St65) for high energy and elementary particle physics applications (Ri74; Sc79). More recent applications (e.g., Ec77; Ro77) have employed image-intensified cameras to view the streamer, allowing the detector to be operated at lower gain with a consequent reduction in streamer track extension. Spatial resolution of $\leq 100 \mu\text{m}$ have been achieved using streamer chambers in recent experiments (Ec84,85), but since these devices are still operated at high gain in

the space-charge region, no information on the electron track density is obtained.

Gas Scintillation Detectors

Direct gas scintillator detectors (e.g., Si84), gas scintillation proportional counters (e.g., Co67; Po67; Al80,81; Si84), and gas scintillation drift chambers (e.g., Ma84) have also been developed. These are similar in principle to the electrical detection schemes described above, except that the energy and position of the electrons in the track are measured by the photon flux and the location of production of the optical radiation in the gas.

Conclusions

This brief description has summarized the major concepts that could be used to image the ionizing radiation particle track in neutron and microdosimetry applications. However, neither the electrical nor optical techniques outlined above have demonstrated at the present time the capability to obtain the three-dimensional distribution of all the secondary electrons in a particle track. This is due primarily to the considerable complexity of the detector chamber and associated electronic amplification techniques required in multiwire proportional and drift chambers and the necessity of operating at high gas amplification (and subsequent space-charge saturation problems) with conventional optical techniques.

CHAPTER 3

OPTICAL IONIZING RADIATION DETECTOR

A technique which does have the capability of directly imaging the electrons in an ionizing radiation track was developed by Cavalleri (Ca69) to determine the number of electrons in a low electron concentration discharge and has been used in recent years to measure the thermal electron diffusion coefficients (Gi73; Rh75a,b; He80b,c), low field electron drift velocity (He80a; Re80), and thermal electron attachment coefficients (Cr83; He83; Pe85) in several gases. This method, coupled with modern two-dimensional digital imaging techniques, is capable of recording the detailed track structure required in microdosimetry applications. The operation of an optical detector of this type is outlined in this chapter, and a sensitivity and resolution analysis of this device under typical operating conditions is given in Chapter 4.

Optical Detector Operation

A schematic diagram of the proposed detector is given in Fig. 2. Ionizing radiation (charged particle, recoil particle, laser beam, etc.) enters the detector through a window or converter material and collides

with a low-pressure ($P \approx 0.1$ to 10 kPa) gas or gas mixture between two parallel metallic electrodes. The gas between the electrodes is ionized in collisions with the high-energy primary radiation and secondary electrons to produce a track of low-energy electrons in the gas. A small continuous RF ($f \approx 10$ to 100 MHz) or DC field ($E/N \approx 0.1$ to 10.0×10^{-17} V cm²; E/N is the density-normalized electric field strength) is applied across the electrodes to "heat" the electrons in the track above thermal energy so as to prevent electron-positive ion recombination from removing electrons before imaging.

The high-energy ionizing radiation and secondary electrons will electronically excite as well as ionize the gas or gas mixture in the chamber, and the prompt decay of these excited atoms or molecules will produce a small burst of optical radiation which can then be detected by two wide angle, fast, high sensitivity photomultipliers. Signals from the photomultipliers are amplified and fed into a fast discriminator-coincidence detector where a trigger pulse is produced when two photomultiplier pulses are detected within a given coincidence window ($T \approx 0$ to 50 ns). This trigger pulse is fed into a master timing circuit which in turn triggers a high voltage (1 to 50 kV) highly damped (decay time $\tau \approx 100$ ns to 1 μ s) RF pulse generator ($f \approx 20$ to 100 MHz). The RF pulse from this generator is applied across the electrodes in the detector and excites the electrons in the particle track.

The RF field causes the electrons to rapidly oscillate, gaining sufficient energy to ionize and electronically excite the surrounding gas and, consequently, to produce a pulse of light whose intensity is directly proportional to the magnitude and duration of the RF pulse. The frequency of the pulse generator is adjusted such that the average

energy of the electrons remains essentially constant during one period of the field (this sets the lower limit on the frequency), but at the same time the electron momentum follows the alternating field (i.e., low enough such that the electron experiences several collisions with the surrounding gas during one period of the field). The gas within the detector is chosen to have a high gas-ionizing efficiency (i.e., low ionization threshold and W value) but more importantly to have a high quantum yield for the production of prompt (decay times ≤ 10 ns) UV to visible (300 to 600 nm) radiation. The amplitude and duration of the RF pulse is chosen such that every electron in the track produces a detectable pulse of light in both of the detector cameras.

The two-dimensional digital detector cameras may either be silicon-intensified vidicon cameras or microchannel plate-intensified charge-coupled device (CCD) or similar semiconductor cameras. These cameras must have large pixel arrays ($>500 \times 500$ pixels) to accurately image the optical radiation produced by the excitation of the electrons in the detector. The resolution of the detector is proportional to the size of the pixel arrays in the camera. The cameras, which are triggered by a pulse from the master timing circuit have variable exposure times which are adjustable (10 ns to 1 μ s) to ensure that at least one detectable photon is recorded by both cameras for every electron in the track. The two cameras image the track in the x-z and y-z planes, and the digitally stored track image is transferred to a computer for permanent storage, track reconstruction, and analysis.

After the imaging of the particle track is complete, a small DC clearing field is applied across the detector electrodes to clear the

electrons and ions from the detector chamber, and the detection circuits are reset to record a second particle track.

CHAPTER 4

DETECTOR DESIGN CRITERIA

The major advantage of this detection technique over the methods outlined in the Introduction is the single electron spatial distribution measurement capabilities of the present method. When the ionizing particle track density is low (a total of a few hundred to a few thousand electrons per track, depending on the gas pressure and rate of ionization in the gas), the three-dimensional spatial distribution of all the electrons can be found to within a given uncertainty. At higher particle track densities, the electron density within a given spatial subvolume can be obtained. The magnitude of the uncertainties in the location of the electrons is discussed below. A further significant advantage of this detection scheme is that the track resolution and detector sensitivity are externally controlled after the chamber has been assembled by manipulation of the gas (species, composition, pressure), RF high voltage pulse (frequency, duration, magnitude), and camera characteristics (aperture size, shutter speed, detector type).

The spatial resolution and sensitivity that can be achieved with this detector in neutron dosimetry and microdosimetry applications is

ultimately governed by the size of the detection volume, the overall quantum efficiency, and spatial resolution of the digital cameras, and the optical, transport, and rate coefficient properties of the gas mixtures used in the detector chamber. In the following analysis, the detector is arbitrarily chosen to have sides 10 cm in length. These dimensions are the same as those used in previous analyses of the digital approach to neutron dosimetry (Tu85a,b; Bo87). The detector camera is also assumed to possess a 500×500 pixel array with single pixel resolution. With these dimensions, the single electron spatial uncertainty is $\pm 200 \mu\text{m}$ in any coordinate. This limiting resolution can, of course, be improved by using smaller detection volumes ($\ll 1 \text{ cm}^3$) or a digital camera with a larger pixel array size. In practice, several other factors govern the maximum resolution that can be achieved by this type of detector. These factors are discussed below.

Photon Gain Requirements

When the RF electric field is applied to the detector chamber, the electrons in the particle track are excited and give off radiation as well as ionize the surrounding gas. This radiation is, to a first approximation, produced isotropically from a small volume (which in this analysis is assumed to be a point source), and only a small fraction of the radiation is imaged by the cameras. When the distance from the source to the imaging optics R (Fig. 2) is much greater than the radius of the imaging lens, r , then the fraction of the photon flux incident upon the lens is

$$\begin{aligned}
 F_L &\approx \frac{\text{area of the lens}}{\text{surface area of the sphere of radius R}} \\
 &= r^2/4R^2 \\
 &= r^2/4f^2 (1 + m)^2 ,
 \end{aligned}$$

where f is the focal length of the lens (Fig. 2) and m is the reduction ratio. The intensity of the radiation incident upon the detector imaging face is increased by the factor m^2 due to the reduced image size of the camera. Consequently, the fraction of the photon flux incident upon the detector is

$$F_D = \frac{Q \rho r^2 m^2}{4f^2 (1 + m)^2} , \quad (1)$$

where ρ is the fraction of the optical radiation transmitted (i.e., not lost by reflection or absorption) through the windows and lens system (typically $\rho \gtrsim 0.8$). The detector sensitivity must also be weighted by the overall quantum efficiency (Q) of the camera, where it is reasonable to assume that when the camera is operated at sufficiently high gain ($\approx 10^4$ to 10^6) all electrons released from the photocathode will produce a recordable signal. The quantum efficiency for SIT vidicon camera systems is $\approx 5\%$ and for MCP-enhanced semiconductor cameras is $\approx 20\%$ over the wavelength range of interest ($\lambda \approx 200$ to 500 nm). An estimate of the minimum total photon flux, ϕ , required from a point source to produce a recordable event in the detector (with a probability of 50%) can be seen from the following example, where if we assume $f = 20$ cm,

$m = 10$ and $r = 2.5$ cm, then $\phi \approx 2 \times 10^3$ photons. In a real radiation detector, only the optical radiation produced at the center of the chamber is in focus (i.e., optimally resolved). Reducing the radius of the imaging optics to $r = 0.5$ cm to improve the depth of focus (i.e., to reduce the uncertainty in the position of production of the radiation near the edge of the detector), then $\phi \approx 5 \times 10^4$ photons. Consequently, we require $\phi \gtrsim 10^5$ photons for each secondary electron if the detector is to image every electron with high probability. This requirement governs the other operating parameters of the detector.

AC Electric Field Requirements

For ease of operation and simplicity of analysis, it is desirable to operate the radiation detector under conditions where the alternating high voltage electric field of the form $E(t) = E_0 \sin \omega t$ (where E_0 is the initial field strength and ω is the angular frequency of the electric field) is equivalent to a constant DC electric field as experienced by the electrons in the particle track (i.e., the transport and rate coefficients of the electrons are time invariant). This requirement leads to the two following conditions. For $E(t)$ to appear to be approximately constant, then the following relation must hold (Ca69)

$$E^2 = E_0^2 (1 + 2\omega^2/v^2)/2, \quad (2)$$

where v is the effective momentum transfer collision frequency. This implies

$$E \approx E_0/2^{1/2} \approx 0.7 E_0. \quad (3)$$

when

$$\omega^2/v^2 \ll 10^{-2} . \quad (4)$$

The effective momentum transfer collision frequency is given approximately by $\nu = N \overline{\sigma_m(v) v}$, where N is the total gas number density, $\sigma_m(v)$ is the momentum transfer collision frequency, and v is the electron velocity. In atomic and molecular gases at electron energies considerably in excess of thermal, then $\nu \approx 10^9$ to 10^{10} s^{-1} over the gas pressure range $P = 0.1$ to 1.0 kPa (0.75 to 7.5 torr) (Hu74). Since $\nu \propto N$, then it follows that operating the detector at higher gas pressures allows higher RF frequencies, ω , to be chosen. In practice, the electrons randomize their momentum in a few collisions, and thus the time required to adjust to an alternating electric field is $\tau \lesssim 10^{-8} \text{ s}$ at these gas pressures. Radiofrequency electric fields with frequencies $f \lesssim 100 \text{ MHz}$ satisfy this requirement.

The second requirement to be satisfied is that the fluctuations in the mean electron energy $\langle \epsilon \rangle = \frac{1}{2} m \overline{v^2}$ due to the oscillating electric field be small compared with $\langle \epsilon \rangle$ (i.e., $\lesssim 10\%$). For atomic gases, the time constant for the mean energy decay, τ_ϵ , is of the order of 10^{-6} s (Hu74) but can be considerably shorter for molecular gases (10^{-7} to 10^{-8} s) over the same pressure range. This condition sets a lower limit on ω which for the gas mixtures considered in this study implies $f \gtrsim 10 \text{ MHz}$. Thus, if the high voltage RF field applied to the detector chamber is within the frequency range $10 < f < 100 \text{ MHz}$, then the transport and rate coefficients of the electrons within the track will be approximately time invariant.

Avalanche Growth

The growth in the Townsend avalanche size and optical emission from the electrons in the particle track can now be calculated from the continuity equation of the electrons in the particle track assuming that the electric field is uniform. The analysis of the electron motion in high-frequency electric fields is simplified by noting that the mean value of the radial gradients in the electron energy distribution function $f(\epsilon, E/N)$ are negligible (Hu74), and consequently the electron diffusion is isotropic and the net electron drift is zero. Thus,

$$\frac{\partial n}{\partial t} + D \frac{\partial^2 n}{\partial r^2} + (v_i - v_a) n = 0 ,$$

where $r^2 = x^2 + y^2 + z^2$, D is the isotropic diffusion coefficient, and v_i and v_a are the ionization and attachment frequencies. The solution to this equation is

$$n(r, t) = \frac{n_0}{(4\pi D)^{3/2}} \exp[-r^2/4Dt] \exp[-(v_a - v_i) t] . \quad (5)$$

which gives the time and spatial evolution of a group of n_0 from a point source. The total photon flux, $\phi(t)$, produced by the local electron avalanche is

$$\frac{d\phi}{dt} = n(t) v_e , \quad (6)$$

where v_e is the electronic excitation collision frequency. Integrating eqn (5) over all spatial coordinates and assuming that electron

attachment processes are negligible, then the total photon flux at time, t , is

$$\phi(t) = n_0 \frac{v_e}{v_i} [\exp(v_i t) - 1] . \quad (7)$$

Assuming that $n_0 = 1$ and substituting $v_e = \beta w$ and $v_i = \alpha w$, where α and β are the unnormalized Townsend ionization and photon production coefficients, respectively, and w is the electron drift velocity, then

$$\begin{aligned} \phi(t) &= \frac{\beta}{\alpha} [\exp(\alpha w t) - 1] \\ &= \frac{\beta/N}{\alpha/N} [\exp([\alpha/N] N w t) - 1] . \end{aligned} \quad (8)$$

Equation (8) enables the total photon flux to be obtained at a given E/N value from a knowledge of α/N , β/N , and w , while eqn (5) enables the total electron growth and the radial growth of the electron swarm or avalanche to be estimated as a function of time. The $1/e$ half width of the swarm from eqn (5) at time, t , is given by $r^2 = 4Dt$. Thus,

$$r(t) = \left[\frac{4wt}{N} \left(\frac{D}{\mu} \right) \left(\frac{E}{N} \right)^{-1} \right]^{1/2} . \quad (9)$$

This expression may be used to estimate the widening or the limiting spatial uncertainty (due to the diffusion as a function of time after the application of the high voltage RF field) in the position of production of the original seed electron in the ionizing particle track.

Although the average drift of the electron swarm in the detector is zero for a constant RF field, the centroid of the electron swarm does shift with each half cycle of the applied field. This creates an additional uncertainty in the production of the optical radiation, and an upper limit on the deviation of the swarm centroid from the initial position of production of the seed electron may be found by using the drift velocity of the electrons at the field E given by eqn (3) (i.e., the average of the applied electric field) during the first half cycle of the applied field. The average swarm centroid shift due to electron drift will be between this value and the source position during all further oscillations of the electric field. The spatial uncertainties due to drift and diffusion of the electrons obtained in this manner are upper limits on the effective detector resolution as the avalanche growth is highly exponential in time (see the calculations in N_2 given below), and most of the electrons, and hence photons, are generated just prior to the closure of the camera shutter.

CHAPTER 5

EXAMPLE DETECTOR RESOLUTION AND SENSITIVITY CALCULATIONS

N₂ as a Counting Gas

To obtain an estimate of the magnitude of the electron and photon growth [eqns (5) and (8)] as a function of time, and the decrease in spatial resolution (i.e., increase in the uncertainty that a photon observed by the digital cameras was produced at the position of production of the initial electron in the particle track) due to electron diffusion [eqn (9)] and drift, sample calculations of these parameters have been performed in N₂. Nitrogen was chosen to illustrate the growth in these parameters, as the relevant electron transport and rate coefficients are readily available, and N₂ has a high production coefficient for near UV light (337 nm from the second positive band C³Π_u-B³Π_g) which both intensified vidicon and solid state cameras can detect with good quantum efficiency. Very strong optical emission from this band has been observed in 10 MHz RF discharges in N₂ (Ha78). Pure N₂ is not necessarily the optimum gas to choose in this application as will be outlined in the Conclusion.

Literature values for the electron ionization coefficient α/N (Ba65; Jo68, Da70, Fo73, Ha76) and the photon production coefficient β/N (Le63) in N_2 are given in Fig. 3, and the electron drift velocity w (Sc65; Bl67; Fl80; We85) and transverse diffusion coefficient (which in this application is equivalent to the isotropic diffusion coefficient) to electron mobility ratio D/μ (Na68; Fl80; Ro80; We85) values are given in Fig. 4 along with the curves (dashed lines) used in the present calculations. The photon production as a function of time for several E/N values and gas pressures has been calculated using eqn (5) along with the data given in Figs. 3 and 4, and the results are shown in Fig. 5. The total photon fluxes (i.e., the total number of photons) obtained after a given time interval at several gas pressures are given in Fig. 6 as a function of the average applied density-normalized electric field strength, E/N . These calculations show the sensitivity of the total rate of photon production to these parameters. In particular, 80 to 90% of the total light produced by the avalanche occurs during the last 20% of the observation time for moderate to high electron multiplication (10^4 to 10^6). The total photon flux is even more sensitive to variations in E/N , and the present calculations indicate that reproducible results will only be achieved in this detector by precise synchronization of the high voltage and camera triggering units, and control of the high voltage field strength and camera shutter opening times. Nevertheless, these calculations do show that large photon fluxes are obtainable with readily obtainable RF field voltages, gas pressures, and camera shutter opening times.

From Chapter 4, a total of $\geq 10^5$ photons are required to image at least one of these photons in each of the digital cameras (Fig. 2). The

effective increase in the spatial uncertainty of the position of production of the optical radiation due to electron diffusion [eqn (9)] (and hence the position of production of the initial seed electron in the particle track) obtained at the time, t , when a total of 10^5 photons have been produced (Fig. 5) is given in Fig. 7 as a function of the gas pressure for several E/N values. These calculations are also shown in comparison with the value of the ultimate detector resolution ($\approx 200 \mu\text{m}$) due to the size of the chamber (10 cm on each side) and the pixel array size (500×500) of the digital cameras.

These calculations indicate that operation of this detector at high E/N values and gas pressures reduces the radial diffusion and hence the uncertainty in the position of the initial seed electron in the particle track. Unfortunately, the initial electron density in the particle track is proportional to the gas pressure and for high-density tracks [e.g., those produced by carbon recoil ions (Fig. 1b)] adequate resolution of the electrons in the track might only be possible at relatively low gas pressures. The present calculations do indicate that for moderate particle track densities (a few electrons per millimeter) it is possible to achieve radial uncertainties of the order of the ultimate resolution ($\approx 200 \mu\text{m}$) possible with the detector in its proposed configuration.

The maximum displacement of the electron avalanche centroid due to drift in the direction of the applied electric field (z direction, Fig. 2) during one half cycle of the RF field is shown in Fig. 8 as a function of the RF field frequency for three E/N values. The points in Fig. 8 indicate the maximum displacement of the swarm that occurs during half the time interval that it takes for the avalanche to grow to a size

such that 10^5 photons are produced at these E/N values and at the gas pressures indicated. The time required for this avalanche growth is independent of the RF field frequency provided E is assumed to be constant and can then be directly obtained from the calculations given in Fig. 5. Operation of the detector at a given gas pressure and at the RF field frequency indicated by the location of the points on the curve for a given E/N value in Fig. 8 means that the swarm will grow to a size such that exactly 10^5 photons are produced during one full cycle of the applied field. This is the optimum operating frequency of the detector for a particular gas pressure and E/N value, since most of the photon production (>90%) occurs during the last 10 to 20% of the avalanche growth time (Fig. 5). Consequently, if radial electron diffusion were negligible, >90% of the photons would then be produced within a volume of radius <20% of the maximum avalanche displacement under these conditions.

CHAPTER 6

CONCLUSIONS AND RECOMMENDATIONS

Further Improvements in Detector Resolution and Sensitivity

A description of an ionizing radiation detector has been given which has the capability of measuring the three-dimensional spatial distribution of all the secondary electrons in the track left by the passage of the ionizing radiation through a low-pressure (0.1 to 10 kPa) gas. The calculations given in the preceding section indicate that when N_2 is used as the fill gas in the detector, a spatial resolution $\leq 1 \text{ mm}^3$ is obtainable for each electron in the particle track. Further improvements in the detector resolution and uniformity of the resolution throughout the detector can be achieved by three-dimensional imaging of the chamber volume using three cameras in a triangular pyramidal configuration. This arrangement has not been analyzed in the present study as the gas characteristics, rather than the camera or chamber characteristics, are thought to limit the ultimate resolution that is achievable with the proposed detector.

The optical emission and resolution characteristics of the detector can be improved more readily by using specially tailored gas mixtures

with optimized rate and transport coefficients. In conventional multiwire proportional and drift chambers low electron diffusion and high electron multiplication rates, combined with high electron drift velocities (proportional counters) or low electron drift velocities (drift chambers) are required gas characteristics. The main gas requirements in the present detector are gas mixtures which have large coefficients for the production of prompt (<50 ns) UV to visible radiation (200 to 500 nm) with high gas multiplication rates and low electron drift velocities and diffusion coefficients over the operating E/N range. Gas mixtures containing 1 to 10% N_2 in Ar (or the other rare gases) promise to possess these characteristics in comparison with pure N_2 . Higher light and charge multiplication factors (A180,81) combined with lower electron drift velocities at high electric field strengths have been observed in N_2 /Ar gas mixtures (Lo76; A180) in comparison with pure N_2 . The enhanced ionization and optical characteristics in this gas mixture are due, partly to the higher mean energies of the electrons in the avalanche at a given E/N value (i.e., fewer vibrational energy loss collisions with N_2) but also due to the efficient transfer of energy from the resonance and metastable electronic states of Ar to the upper $C^3\Pi_u$ of N_2 (e.g., St64). The energy transfer from excited Ar to N_2 has been shown to be very efficient and has been used in electron-beam-pumped laser studies in Ar/ N_2 gas mixtures (e.g., Au74; Se74a,b). Penning ionization gas mixtures (e.g., Ri74) can also be used to produce additional ionization in the gas rather than additional optical radiation. Both processes have the net result of increasing the optical emission from the avalanche. The proposed technique, combined with recently available fast-imaging techniques is a considerable improvement

over previous optical detection methods where in the present scheme gas amplification of the order 10^4 to 10^6 is required to image the electrons which can be compared with amplification factors $>10^8$ to 10^9 which are required in conventional streamer detectors using photographic detection methods (Ri74).

Advantages of the Optical Detector Concept

The resolution obtainable with the present detector may also be compared with the $\lesssim 100 \mu\text{m}$ uncertainty using the more sophisticated multiwire proportional and drift counters described in the Introduction. Although these counters can locate the position of the particle track in the counter with high resolution, they have yet to demonstrate the capability of measuring the initial charge distribution with the particle track with the sensitivity required for microdosimetry applications. The present technique has the capability of obtaining good spatial resolution with excellent charge distribution measurement which are essential in neutron dosimetry and microdosimetry (Tu85a,b; Bo87).

A further advantage of the present technique is the comparative simplicity of the detector chamber and the associated imaging electronics in comparison with high precision multiwire chambers where high machining and manufacturing tolerances are required associated with complex signal amplification and processing. The operating conditions of the present detector are all externally controllable over a wide range of parameters, such that optimization of the detector characteristics is readily accomplished depending upon the energy and type of ionizing radiation being detected. The major performance limitation of the detector is the relatively low ionizing radiation

detection rate (<10 to 100 events per second) which is due primarily to the necessity to transfer, store, and analyze the very large amounts of data that are acquired during the imaging of each ionization event. The resolution and performance of this device is ultimately limited by the transport and rate coefficient characteristics of the fill gas in the chamber and the pixel array size, sensitivity, and image processing capabilities of the digital cameras and can be improved by the ongoing technological advances in these fields.

REFERENCES

- Al80 Al-Dargazelli S. S., Ariyaratne T. R., Breare J. M. and Nandi B. C., 1980, "Measurement of the drift velocity of electrons in an argon-nitrogen mixture using a gas scintillation drift chamber," *Nucl. Instrum. Meth.* **176**, 523.
- Al81 Al-Dargazelli S. S., Ariyaratne T. R., Breare J. M. and Nandi B. C., 1981, "Charge and light gain measurements in argon-nitrogen mixtures using a gas scintillation proportional counter," *Nucl. Instrum. Meth.* **180**, 497.
- Au74 Ault E. R., Bhaumik M. L. and Olson N. T., 1974, "High-power Ar-N₂ transfer laser at 3577 Å," *IEEE J. Quantum Electronics* **QE-10**, 62.
- Ba65 Bagnall F. T. and Haydon S. C., 1965, "Pre-breakdown ionization in molecular nitrogen in E x B fields," *Aust. J. Phys.* **18**, 227.
- Ba85a Bateman J. E., 1985, "The pin detector - a simple, robust, cheap and effective nuclear radiation detector," *Nucl. Instrum. Meth.* **A238**, 524.
- Ba85b Bateman J. E., 1985, "The imaging pin detector," *Nucl. Instrum. Meth.* **A240**, 177.
- B167 Blevin H. A. and Hasan M. Z., 1967, "The drift velocity of electrons in nitrogen," *Aust. J. Phys.* **20**, 741.
- Bo68 Borkowski C. J. and Kopp M. K., 1968, "New type of position-sensitive detectors of ionizing radiation using risetime measurement," *Rev. Sci. Instrum.* **39**, 1515.
- Bo86 Bolch W. E., Turner J. E., and Hamm R. N., 1986, "An algorithm for unfolding neutron dose and dose equivalent from digitized recoil-particle tracks," Oak Ridge National Laboratory Report ORNL/TM-10168.
- Bo87 Bolch W. E., Turner J. E., Hamm R. N., Hurst G. S. and Wright H. A., 1987, "A method of obtaining neutron dose and dose equivalent from digital measurements and analysis of recoil-particle tracks," *Health Physics* (in press).

- Bu65 Bulos F., Boyarski A., Diebold R., Richter B., Odian A. and Villa F., 1965, "Development of streamer spark chambers," *IEEE Trans. Nucl. Sci.* NS-12, 22.
- Ca69 Cavalleri, G., 1969, "Measurements of lateral diffusion coefficients and first Townsend coefficients for electrons in helium by an electron-density sampling method," *Phys. Rev.* 179, 186.
- Ch57 Charpak G., 1957, "Principe et essais preliminaires d' un nouveau detecteur permettant de photographier la trajectoire de particules ionisantes dans un gaz," *J. Phys. Rad.* 18, 539.
- Ch64 Chikovani G. E., Roinishvili V. N. and Mikhailov V. A., 1964, "Operation mechanism of the track spark chamber," *Nucl. Instrum. Meth.* 29, 261.
- Ch68 Charpak G., 1968, "The use of multiwire proportional counters to select and localize charged particles," *Nucl. Instrum. Meth.* 62, 262.
- Ch70 Charpak G., 1970, "Evolution of the automatic spark chambers," *Ann. Rev. Nucl. Sci.* 20, 195.
- Ch79 Charpak G. and Sauli F., 1979, "Multiwire proportional chambers and drift chambers," *Nucl. Instrum. Meth.* 162, 405.
- Co60 Colli L., Fazio M. and Rossini T., 1960, "The discharge chamber developed as an alpha particle detector," *Energia Nucleare* 7, 865.
- Co67 Conde C.A.N. and Policarpo A.J.P.L., 1967, "A gas proportional scintillation counter," *Nucl. Instrum. Meth.* 53, 7.
- Co80 Comby G., Mangeot Ph., Prugne P., Chalot J. F., Coulareau E., Quidort J., Beauval J. J. and Tichit J., 1980, "Multi-needle detector with cathode focusing," *Nucl. Instrum. Meth.* 176, 313.
- Cr83 Crompton R. W. and Haddad G. N., 1983, "Thermal electron attachment to SF₆ and CFC₃," *Aust. J. Phys.* 36, 15.
- Da70 Daniel T. N. and Harris F. M., 1970, "The spatial growth of ionization currents in nitrogen at voltages up to 500 kV," *J. Phys. B* 3, 363.
- Do64 Dolgoshein B. A., Rodionov B. U. and Luchkov B. I., 1964, "Streamer chamber," *Nucl. Instrum. Meth.* 29, 270.
- Ec77 Eckardt V., Seyboth P., Derado I., Gebauer H.-J., Odian A. and Pretzl K. P., 1977, "Particle identification in a large streamer chamber with reduced memory time," *Nucl. Instrum. Meth.* 143, 235.
- Ec84 Eckardt V., Lecoq P., Wenig S. and Wiatrowski E., 1984, "A holographic high pressure streamer chamber," *Nucl. Instrum. Meth.* 225, 651.

- Ec85 Eckardt V. and Wenig S., 1985, "Dark field illumination as a recording technique in a high pressure streamer chamber," *Nucl. Instrum. Meth.* A234, 606.
- Fa80 Fabjan C. W. and Fischer H. G., 1980, "Particle detectors," *Rep. Prog. Phys.* 43, 1003.
- F180 Fletcher J. and Reid, I. D., 1980, "The transport parameters of an electron swarm in nitrogen at elevated E/N," *J. Phys. D* 13, 2275.
- Fo73 Folkard M. A. and Haydon S. C., 1973, "Experimental investigations of ionization growth in nitrogen: 1," *J. Phys. B* 6, 214.
- Fu59 Fukui S. and Miyamoto S., 1959, "A new type of particle detector: the 'Discharge Chamber'," *Nuovo Cimento* 11, 113.
- Fu75 Fujita Y., Taguchi Y., Imamura M., Inoue T. and Tanaka S., 1975, "A low-level needle counter," *Nucl. Instrum. Meth.* 128, 523.
- Fu79 Fulbright H. W., 1979, "Ionization chambers," *Nucl. Instrum. Meth.* 162, 21.
- Gi73 Gibson D. K., Crompton R. W. and Cavalleri G., 1973, "Measurements of the thermal diffusion coefficient for electrons in helium," *J. Phys. B* 6, 1118.
- Gr74a Grunberg C. and Devehat J. Le., 1974, "The needle chamber: A new type of x-y detector using the properties of gaseous multiplication," *IEEE Trans. Nucl. Sci.* NS-21, 89.
- Gr74b Grunberg C. and Devehat J. Le., 1974, "The needle chamber: A new highly versatile detector," *Nucl. Instrum. Meth.* 118, 457.
- Ha76 Haydon S. C. and Williams O. M., 1976, "Combined spatial and temporal studies of ionization growth in nitrogen," *J. Phys. D* 9, 523.
- Ha78 Haydon S. C. and Plumb I. C., 1978, "Time-resolved studies of the electrical breakdown of a gas at radio frequencies," *J. Phys. D* 11, 1721.
- He80a Hegerberg R. and Reid I. D., 1980, "Electron drift velocities in air," *Aust. J. Phys.* 33, 227.
- He80b Hegerberg R., Elford M. T. and Crompton R. W., 1980, "Temperature dependence of the diffusion coefficient for thermal electrons in carbon dioxide over the range 296-468 K," *Aust. J. Phys.* 33, 985.
- He80c Hegerberg R. and Crompton R. W., 1980, "The diffusion coefficient for thermal electrons in mercury vapour at 470 K," *Aust. J. Phys.* 33, 989.

- He83 Hegerberg R. and Crompton R. W., 1983, "Diffusion, attachment and attachment cooling of thermal electrons in oxygen and oxygen mixtures," *Aust. J. Phys.* 36, 831.
- Hu74 Huxley L.G.H. and Crompton R. W., 1974, *The Diffusion and Drift of Electrons in Gases*, pp. 250-253 (New York: Wiley-Interscience).
- Jo68 Jones J., 1968, "Ionization coefficients in nitrogen," *J. Phys. D* 1, 769.
- Le63 Legler W., 1963, "Anregung von UV-strahlung in Stickstoff und Wassestoff durch einen elektronenschwarm," *Z. Physik* 173, 169.
- Lo76 Long W. H., Bailey W. F. and Carscadden A., 1976, "Electron drift velocities in molecular-gas-rare-gas mixtures," *Phys. Rev. A* 13, 471.
- Ma84 Mathis K. D., Simon M. and Henkel M., 1984, "A gas scintillation drift chamber for heavy ion detection," *Nucl. Instrum. Meth.* 225, 407.
- Na68 Naidu M. S. and Prasad A. N., 1968, "The ratio of diffusion coefficient to mobility for electrons in nitrogen and hydrogen," *J. Phys. D* 1, 763.
- Pe85 Petrovic Z. Lj. and Crompton R. W., 1985, "Thermal-electron attachment to SF₆ at room temperature and 500 K," *J. Phys. B* 17, 2777.
- Po67 Policarpo A.J.P.L., Alves M.A.F. and Conde C.A.N., 1967, "The argon-nitrogen proportional scintillation counter," *Nucl. Instrum. Meth.* 55, 105.
- Re80 Reid I. D. and Crompton R. W., 1980, "The drift velocity of low energy electrons in oxygen at 293 K," *Aust. J. Phys.* 33, 215.
- Rh75a Rhymes T. and Crompton R. W., 1975, "Experimental observations of the diffusion cooling of electrons in argon," *Aust. J. Phys.* 28, 675.
- Rh75b Rhymes T., Crompton R. W. and Cavalleri G., 1975, "Diffusion coefficient for thermal electron in neon at 293 K," *Phys. Rev. A* 12, 776.
- Ro77 Rohrbach F., Cathenoz M., Jenny J., Colas J., Fournier D., Noppe J. M and Viellet J. J., 1977, "Hydrogen streamer chamber up to atmospheric pressure," *Nucl. Instrum. Meth.* 141, 229.
- Ro78 Roznerski W., 1978, "The ratio of lateral diffusion coefficient to mobility for electrons in hydrogen and nitrogen," *J. Phys. D* 11, L197.
- Sa75 Sanada J. and Fujita Y., 1975, "Pulse shape from counters with gaseous multiplication," *Nucl. Instrum. Meth.* 131, 469.

- Sa78 Sauli F., 1978, "Limiting accuracies in multiwire proportional and drift chambers," *Nucl. Instrum. Meth.* 156, 147.
- Sc65 Schlumbolm H., 1965, "Messung der driftgeschwindigkeiten von elektronen und positiven ionen in gasen," *Z. Physik* 182, 317.
- Sc79 Schroeder L. S., 1979, "Streamer chambers - their use for nuclear science experiments," *Nucl. Instrum. Meth.* 162, 395.
- Se74a Searles S. K. and Hart G. A., 1974, "Laser emission at 3577 and 3805 Å in electron-beam-pumped Ar-N₂ mixtures," *Appl. Phys. Lett.* 25, 79.
- Se74b Searles S. K., 1974, "Superfluorescent laser emission from electron-beam-pumped Ar-N₂ mixtures," *Appl. Phys. Lett.* 25, 735.
- Si84 Sims M. R., Peacock, A. and Taylor B. G., 1984, "The gas scintillation proportional counter," *Nucl. Instrum. Meth.* 221, 168.
- St64 Strickler T. D. and Arakawa E. T., 1964, "Optical emission from argon excited by alpha particles: Quenching studies," *J. Chem. Phys.* 41, 1783.
- St65 Strauch K., 1965, "Innovations in visual spark chamber techniques," *IEEE Trans. Nucl. Sci.* NS-12, 1.
- Tu85a Turner J. E., Hamm R. N., Hurst G. S. and Wright H. A., 1985, "A digital approach to neutron dosimetry and microdosimetry," in *Proc. 5th Symposium on Neutron Dosimetry, 17-21 September 1984, Munich, FRG* (edited by M. Schraube, G. Burger and J. Booz), Commission of the European Communities, Luxembourg, p. 675.
- Tu85b Turner J. E., Hamm R. N., Hurst G. S., Wright H. A. and Chiles M. M., 1985, "Digital characterisation of particle tracks for microdosimetry," *Rad. Protection Dosimetry* 13, 45.
- Va86 Va'vra J., 1986, "High resolution drift chambers," *Nucl. Instrum. Meth.* A244, 391.
- We85 Wedding A. B., Blevin H. A. and Fletcher J., 1985, "The transport of electrons through nitrogen gas," *J. Phys. D* 18, 2361.

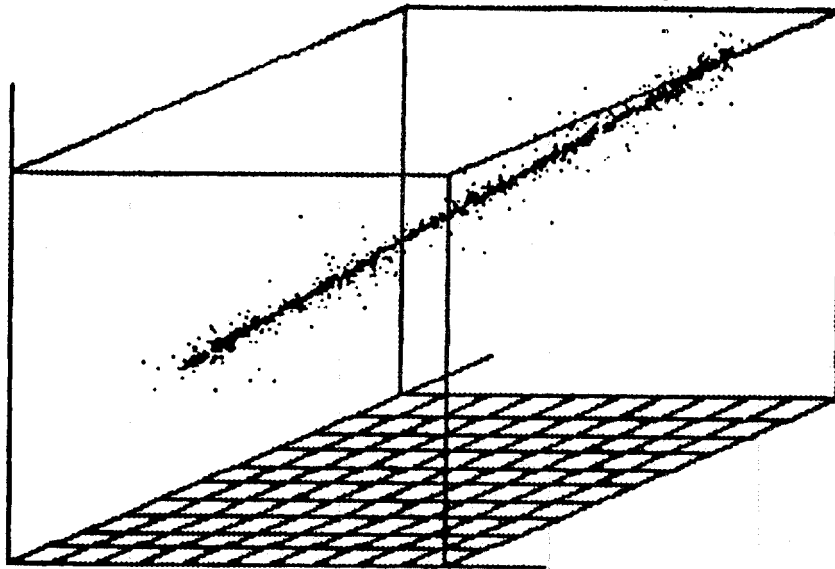


Fig. 1a

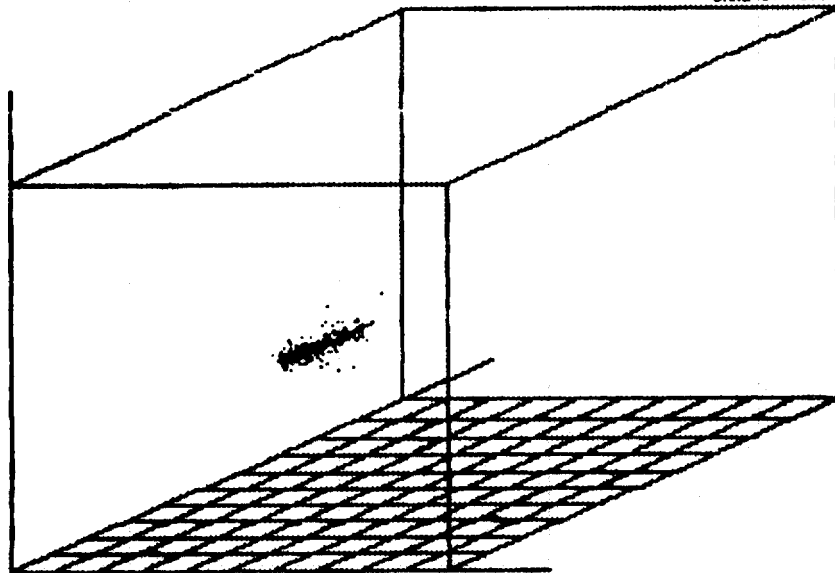


Fig. 1b

Fig. 1. Simulated ionization tracks produced in 1.36 kPa of CH_4 by (a) a 500-keV proton and (b) an 80-keV carbon ion using a charged particle transport code [Bo86.87].

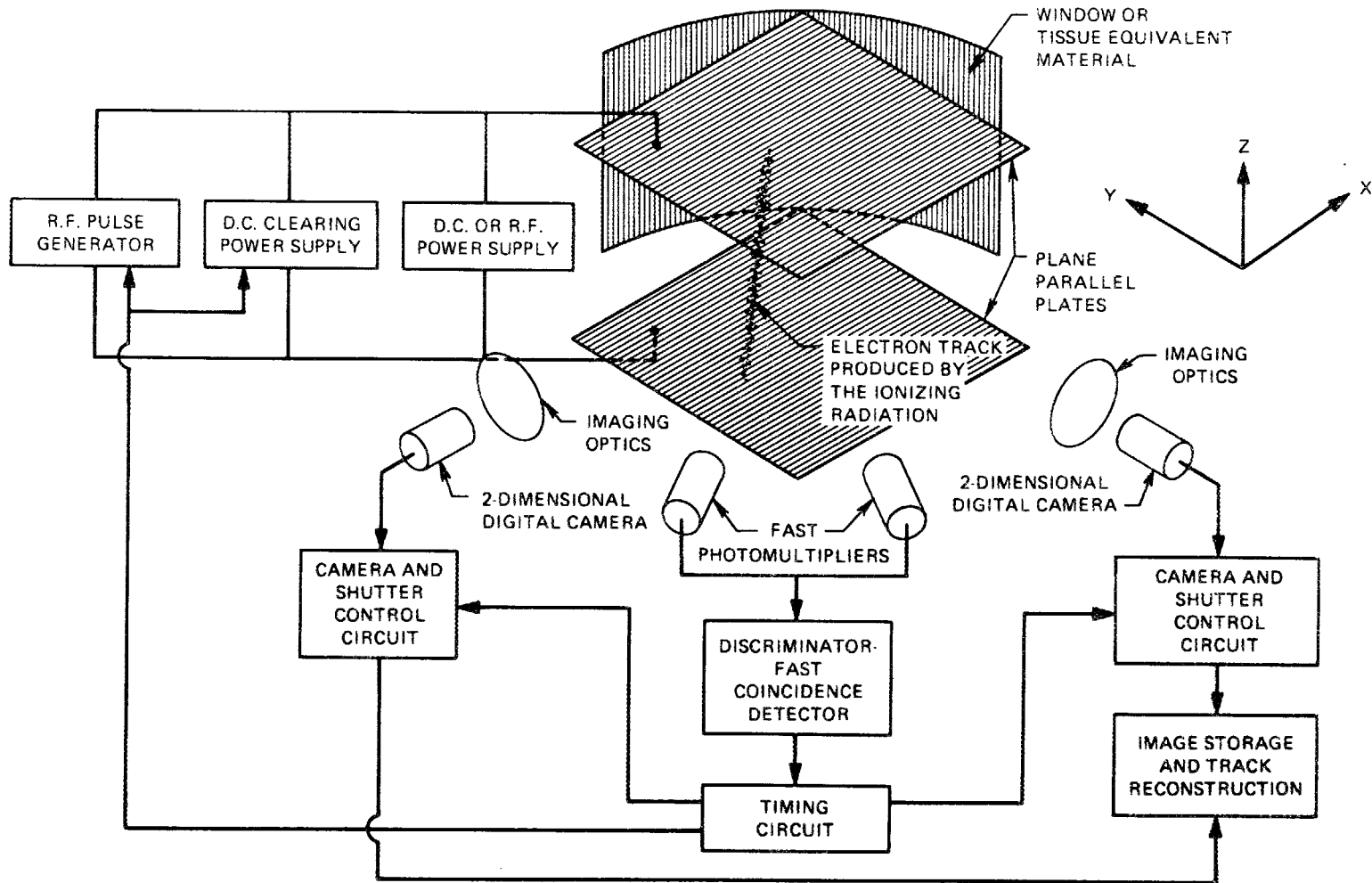


Fig. 2. Schematic diagram of the proposed optical ionizing radiation detector.

ORNL-DWG 86-14101

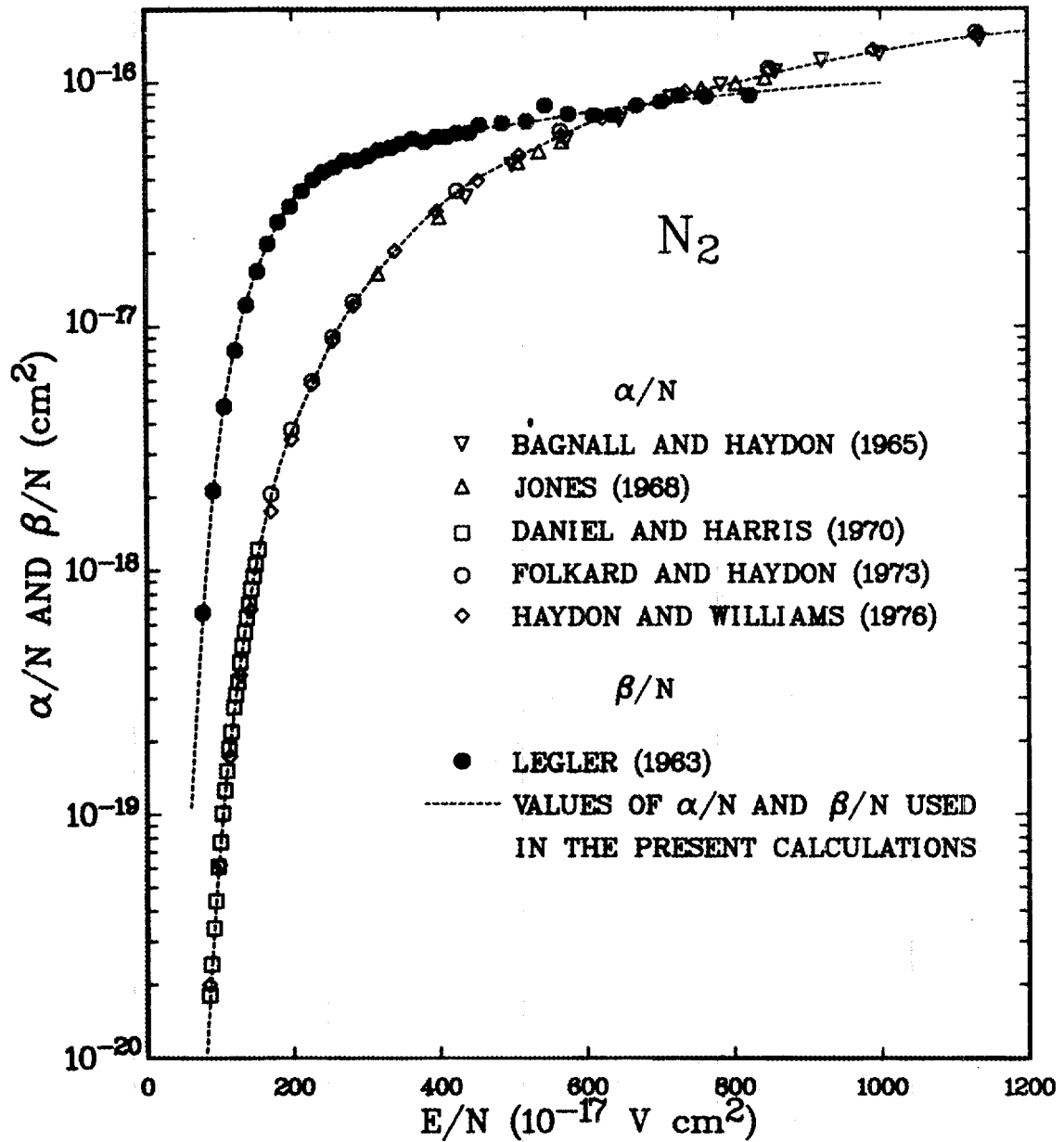


Fig. 3. The electron ionization coefficients, α/N , and photon production coefficients, β/N , for N_2 as a function of E/N . The dashed lines are the values used in the present calculations.

ORNL-DWG 86-14096

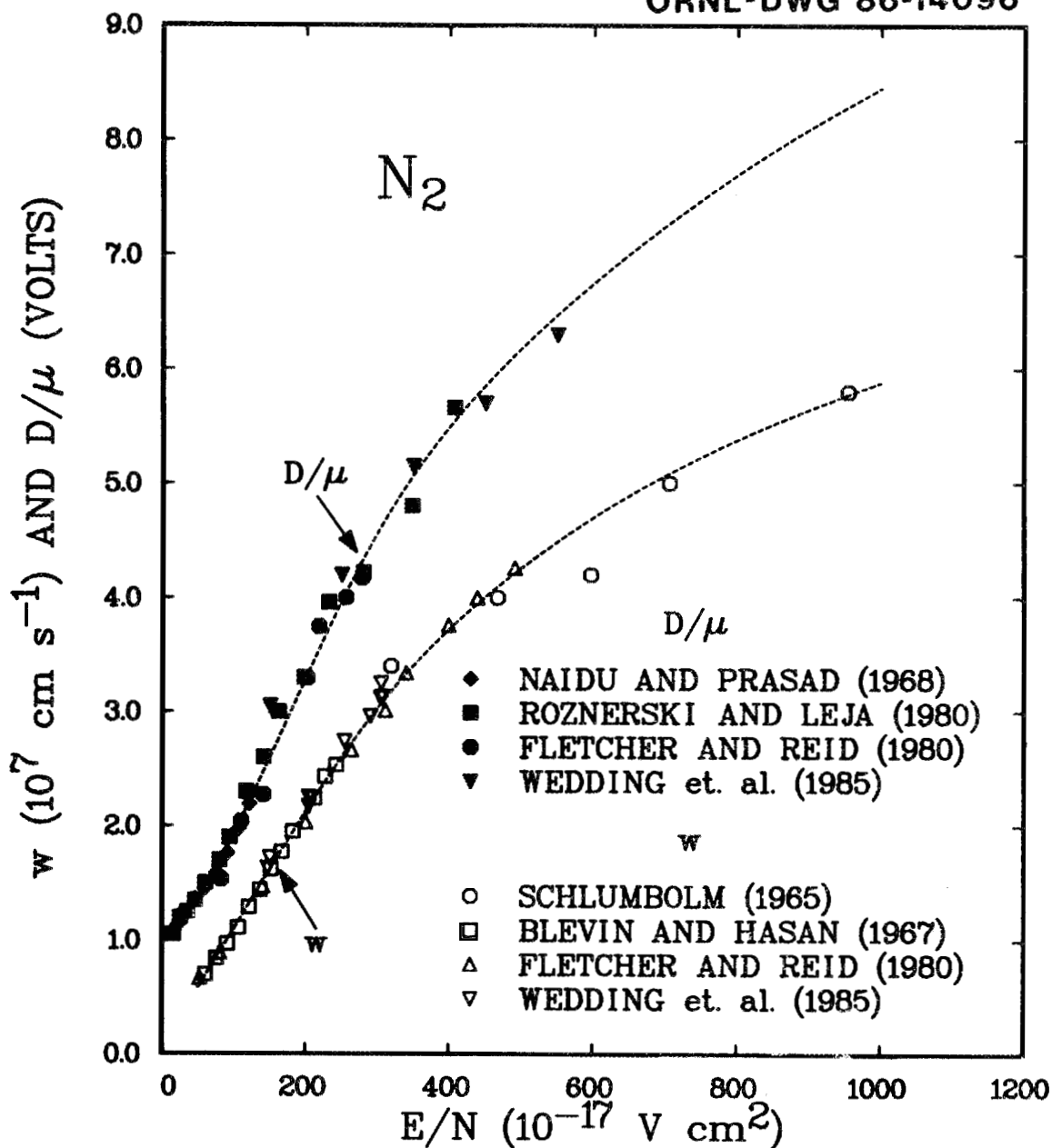


Fig. 4. The electron drift velocity, w , and transverse (isotropic) diffusion coefficient to electron mobility ratio, D/μ , for N_2 as a function of E/N . The dashed lines are the values used in the present calculations.

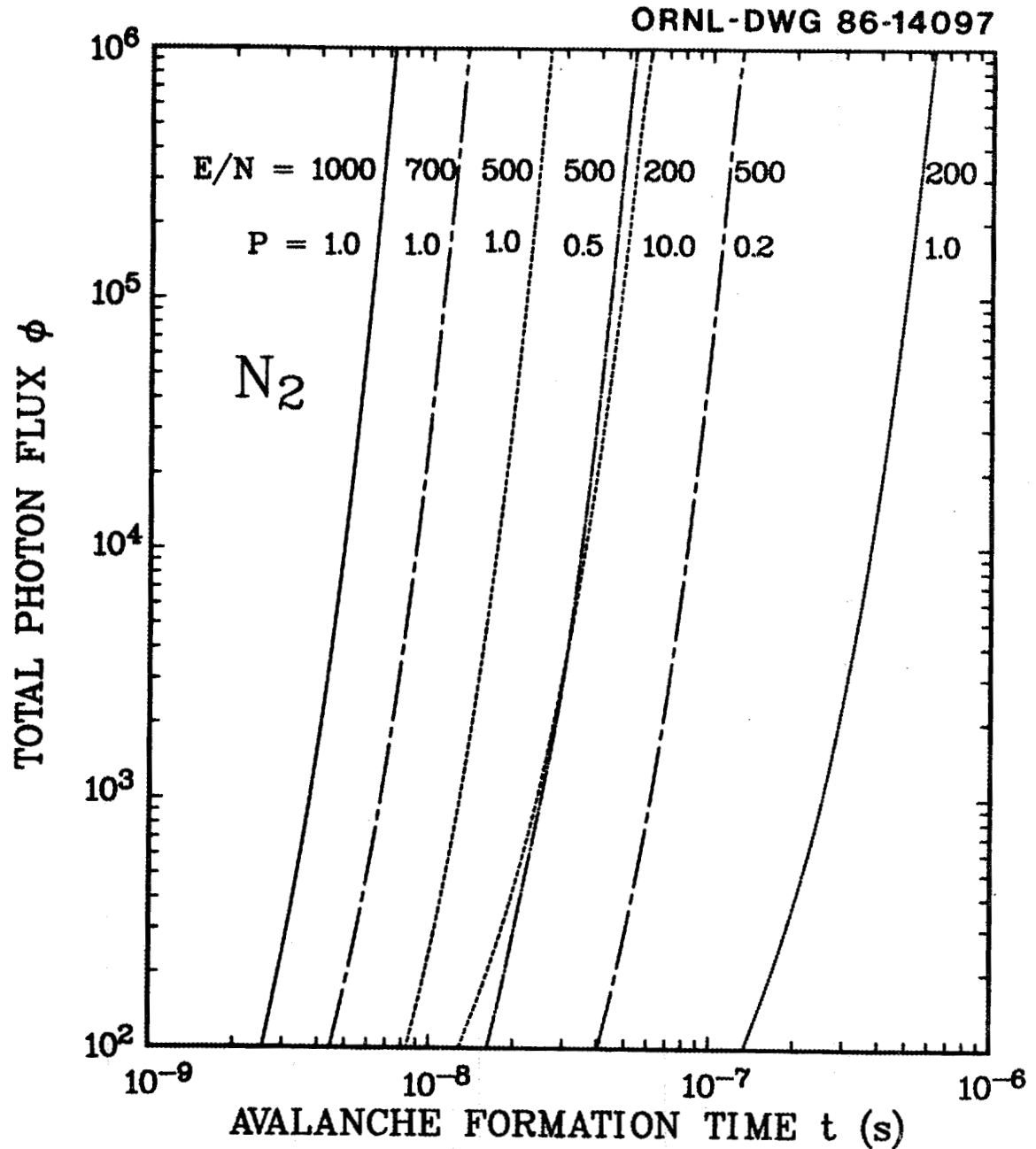


Fig. 5. The total photon flux, ϕ , produced as outlined in the text for N_2 as a function of time after the application of the RF electric field for several E/N values and gas pressures.

ORNL-DWG 86-14098

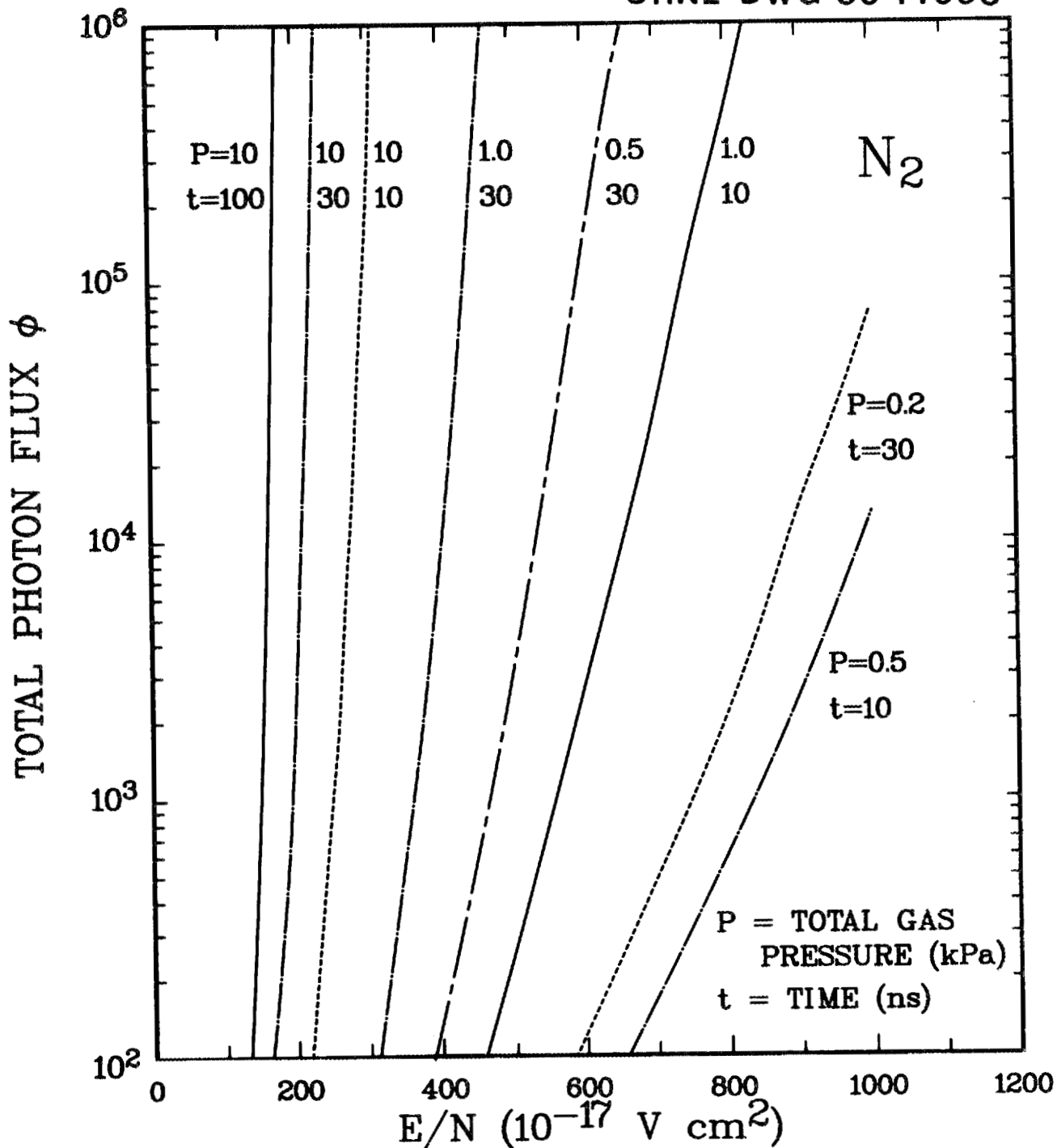


Fig. 6. The total photon flux, ϕ , in N_2 plotted as a function of E/N for several gas pressures and times after the application of the high voltage RF electric field.

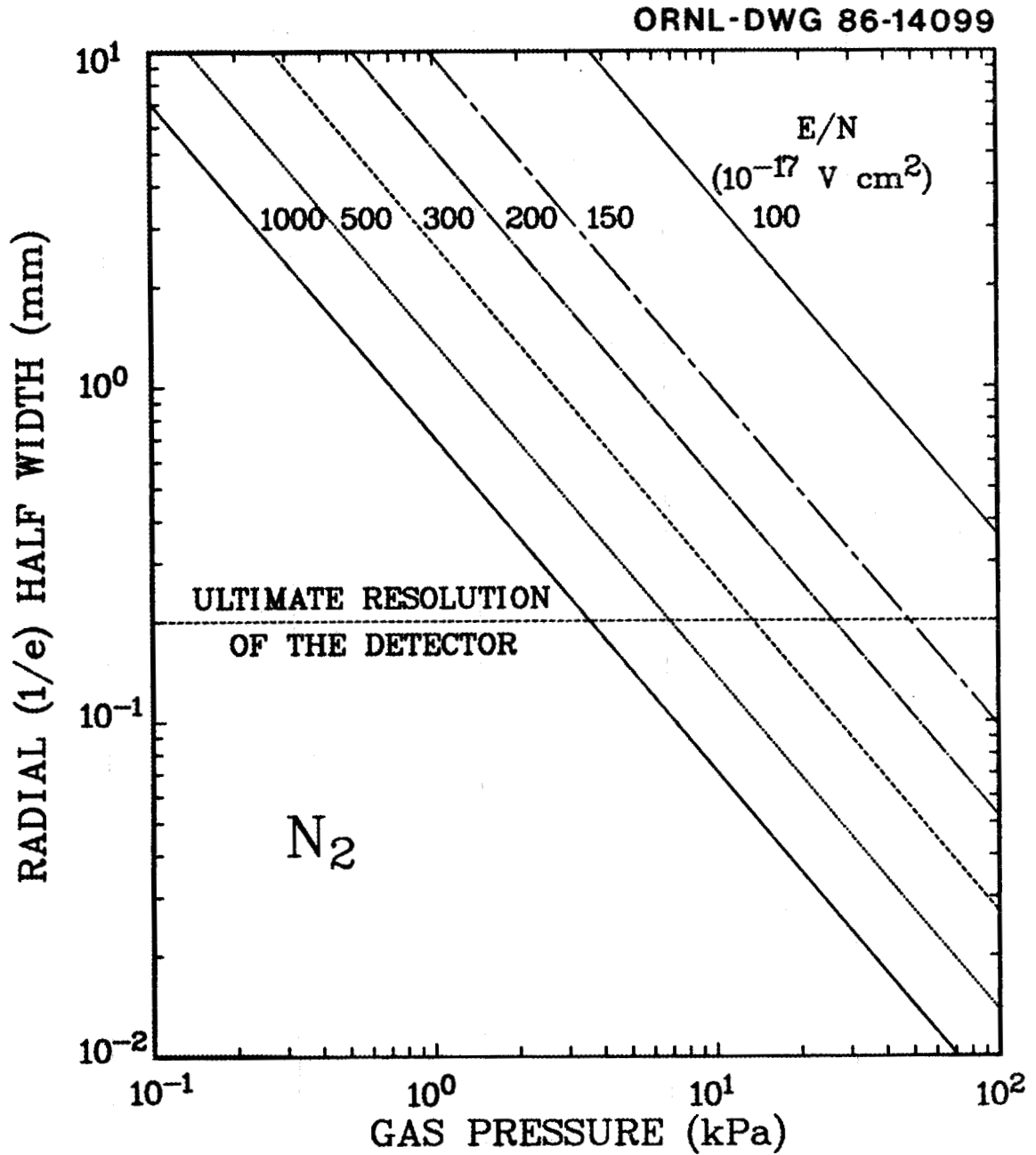


Fig. 7. The (1/e) radial half width of the electron avalanche as a function of the gas pressure in N_2 for several E/N values obtained at the time when a total of 10^5 photons have been produced in the avalanche. The ultimate resolution of the proposed detector is also shown.

ORNL-DWG 86-14100

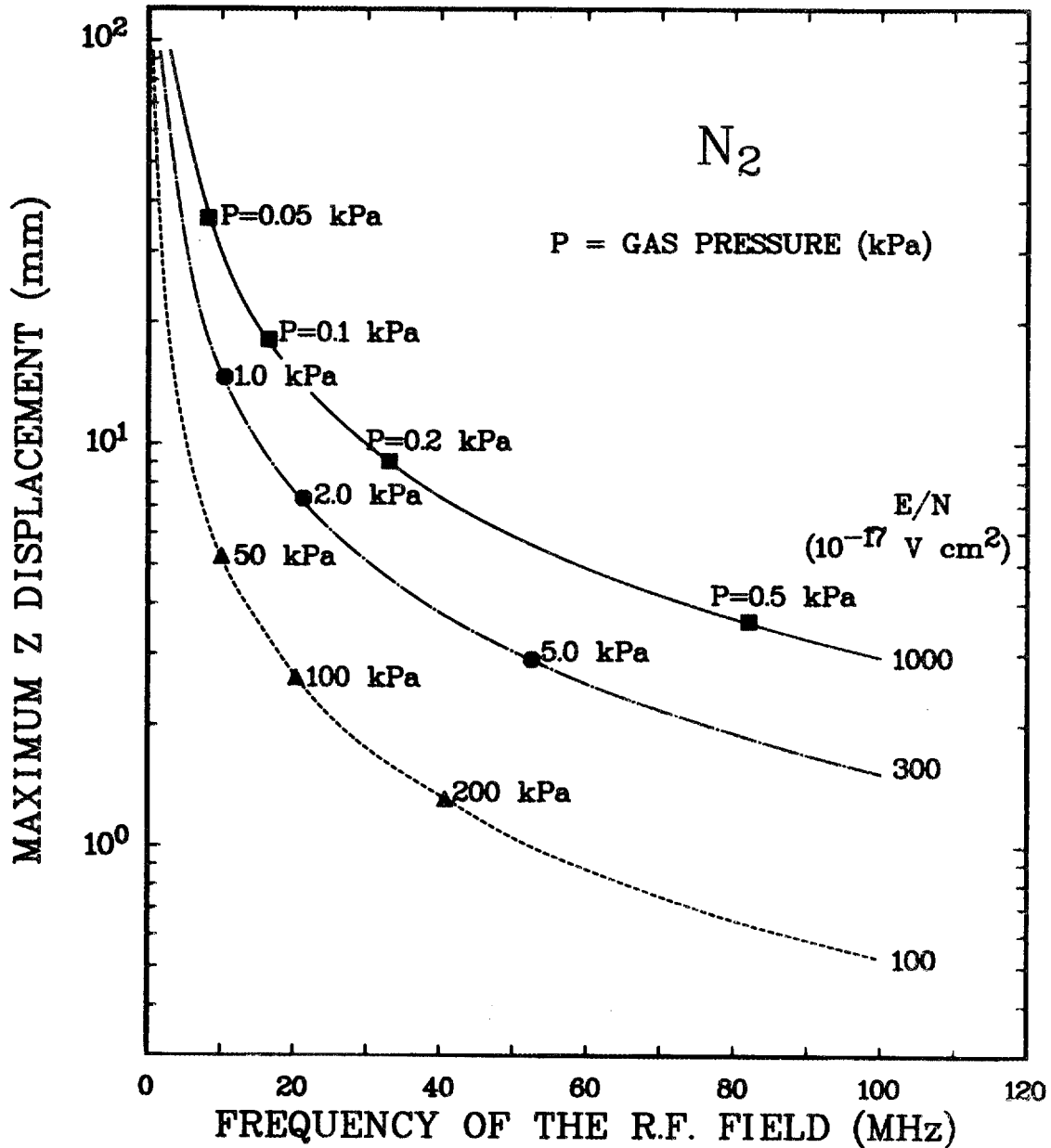


Fig. 8. The maximum avalanche displacement in the field direction due to the drift of the avalanche in N_2 as a function of the frequency of the applied RF electric field. The point on a line at a given E/N value is the operating frequency and gas pressure at which exactly 10^6 photons are produced during one complete cycle of the RF electric field.

ORNL/TM-10421

INTERNAL DISTRIBUTION

1- 2	W. E. Bolch
3	M. M. Chiles
4- 5	R. N. Hamm
6-16	S. R. Hunter
17	C. S. Sims
18	R. E. Swaja
19-20	J. E. Turner
21-22	H. A. Wright
23	Central Research Library
24	Document Reference Section
25-26	Laboratory Records Department
27	Laboratory Records Department-RC
28	ORNL Patent Office

EXTERNAL DISTRIBUTION

29-30	G. S. Hurst, Inst. of RIS, 10521 Research Dr., Suite 300, Knoxville, TN 37932
31	W. M. Lowder, Environmental Measurements Laboratory, U.S. Dept. of Energy, 376 Hudson St., New York, NY 10014.
32	H. G. Paretzke, GSF-Institut fur Strahlenschutz, D-8042 Neuherberg, FRG.
33	H. H. Rossi, Radiological Research Laboratory, Columbia Univ., 630 W. 168th St., New York, NY 10032.
34	R. W. Wood, Office of Health and Environmental Research, U.S. Dept. of Energy, Washington, DC 20545.
35	Office of Assistant Manager for Energy Research and Development, DOE/ORO.
36-37	Technical Information Center, Oak Ridge, TN 37831.

